High detectivity ITO/organolead halide perovskite Schottky photodiodes

Wen Luo[1,4], Lizhi Yan[1,4], Rong Liu[1], Taoyu Zou[1], Shengdong Zhang[1], Chuan Liu[2], Qing Dai[3], Jun Chen[2] and Hang Zhou[1]

[1] School of Electronic and Computer Engineering, Peking University Shenzhen Graduate School, Shenzhen, 518055, People's Republic of China
[2] State Key Laboratory of Optoelectronic Materials and Technologies, School of Electronics and Information Technology, Sun Yat-Sen University, Guangzhou, 510006, People's Republic of China
[3] National Center for Nanoscience & Technology, Chinese Academy of Sciences, Beijing 100190, People's Republic of China

E-mail: zhouh81@pkusz.edu.cn

Abstract

Schottky photodiodes, which are based on metal-semiconductor junctions, are one of the most widely used technologies for low cost image sensor arrays. Here, we fabricate a hole transport layer free organolead halide perovskite diode (ITO/$CH_3NH_3PbI_3$/PCBM/BCP/Ag), and explore its Schottky diode behavior. A Schottky barrier is identified between the transparent conductor ITO and the solution processed perovskite ($CH_3NH_3PbI_3$), with a barrier height of ~0.97 eV measured by capacitance-voltage (C-V) measurements. The Schottky barrier at the ITO/$CH_3NH_3PbI_3$ junction is found to effectively suppress electron injection from ITO to the perovskite under reversed bias, leading to a surprising low dark current of 1.9×10^{-9} A cm^{-2} when biased at −0.1 V. When functioning as a photodetector, the ITO/$CH_3NH_3PbI_3$ Schottky diode outperforms the conventional perovskite photodiode with PEDOT:PSS layer in terms of detectivity, reaching a high specific detectivity (D^*) of 8.9×10^{12} Jones. Moreover, by tuning the band gap of perovskite with the content of bromine (Br), i.e. $CH_3NH_3Pb(I_{1-X}Br_X)_3$($0 \leqslant x \leqslant 1$), the Schottky barrier height at the ITO/perovskite junction is raised, further lowering the dark current of the perovskite photodiode. This work provides fundamental investigation on the device physics of the perovskite Schottky diode, as well as a low cost approach for designing the high sensitivity of photodetectors.

Supplementary material for this article is available online

Keywords: organolead halide perovskite, Schottky photodiodes, dark current, Schottky barrier

(Some figures may appear in colour only in the online journal)

Photodetectors are key components for realizing a wide range of industrial and scientific applications, such as optical communication, medical diagnosis and industrial inspection. Various photodetectors based on inorganic materials, such as ZnO, a-Si:H and GaAs, for applications ranging from UV to NIR detection have been developed in the past [1–3]. For example, an a-Si:H photodiode with an intrinsic layer sandwiched between p-doped and n-doped layers (p-i-n structure) is frequently used in flat panel x-ray imaging [4]. Recently, hybrid organic-inorganic perovskites ($MAPbX_3$, MA short for CH_3NH_3, X = I, Br or Cl) have also become a promising alternative for photodetector applications, due to their outstanding optoelectronic properties, such as tunable bandgap, high absorption coefficient, high charge carrier mobility, and long carrier diffusion length [5–7]. The bandgap of perovskite can be tuned by mixing halide elements in the perovskite [8], usually denoted as $MAPb(I_{1-X}Br_X)_3$($0 \leqslant x \leqslant 1$), which enables the design of photodetectors for a specific wavelength

[4] These authors contributed equally to this work.

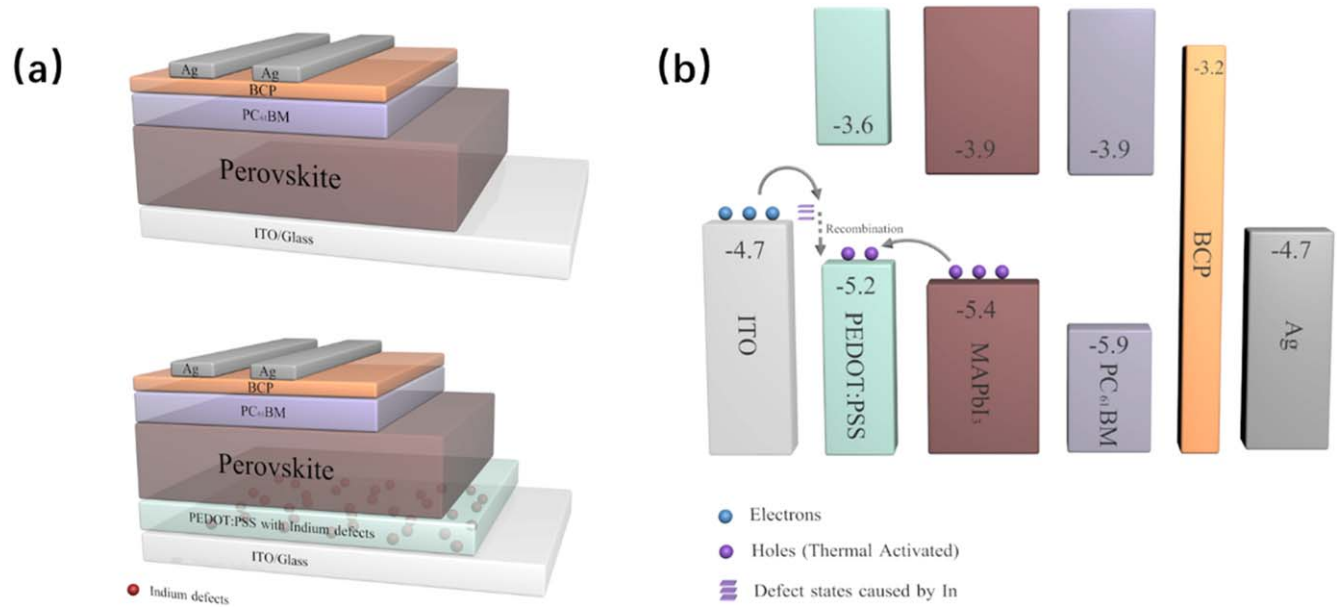

Figure 1. (a) Schematics of $MAPbI_3$ photodetector. (b) Schematic band diagram of each layer in the device before contact, and the proposed electron-hole recombination mechanism in the dark.

range. What makes perovskite materials more attractive is their low temperature solution process ability, which would potentially bring down manufacturing costs and offer flexibility for electronic product design [9, 10].

In general, the photodetectors based on organolead halide perovskite can be divided into two types: photodiode structures (such as a p-i-n structure), and photoconductor structures [11, 12]. The photoconductor type diode offers high photocurrent gain with short channel design [13]. Nonetheless, this type of photodetector is not suitable for applications where a low dark current is required. As for the photodiode structure, most of the reported devices adopted a p-i-n structure similar to its solar cell counterpart (ITO/PEDOT:PSS/perovskite/PCBM/bathocuprione (BCP)/Ag), which has been reported with remarkable power conversion efficiencies of above 20% [14–16]. In the photodiode configuration, it is important to create an asymmetric electrode or electrode interfacial layer at the two terminals for selective carrier transportation. Under dark conditions, the asymmetric electrode arrangement could help reduce the dark current by blocking the thermal activated free carriers. To improve the device performance, several groups have developed different types of hole/electron blocking layers for photodetector applications, including PEDOT:PSS, PTAA and OTPD [17, 18]. An alternative low cost effective way to achieve a low dark current is to adopt a Schottky diode structure. For Schottky contact, the Schottky barrier created at the semiconductor side of the metal-semiconductor interface can block the injection of the carrier under reversed bias, and effectively reduce the dark current of photodetectors. In fact, a typical ITO/a-Si:H schottky diode gives a reasonably low dark current density of $10^{-8} \sim 10^{-9}$ A cm^{-2} when biased at -2 V, and a fair on/off rectification ratio of 10^3 at ± 2 V [19]. Nonetheless, the Schottky diode based on perovskite materials has rarely been reported. The band bending at the metal/perovskite or ITO/perovskite interface has usually been overlooked in previous studies.

Here, a hole transport layer (HTL) free type device with an ITO/perovskite/PCBM/BCP/Ag structure (figure 1(a)) is fabricated, and its photodetection performance is compared to a conventional perovskite photodiode with p-type PEDOT:PSS layer. A schematic band diagram of each layer in the device before contact is shown in figure 1(a), with energy levels similar to previous reports [20, 21]. Our investigation identifies that a Schottky barrier is formed at the ITO/perovskite interface, which effectively suppresses the electron injection from ITO to the perovskite under reversed biased in the dark, leading to a satisfactory low dark current for photodetection applications. As a result, the photodiode without a PEDOT:PSS layer shows a much lower dark current (1.9×10^{-9} A cm^{-2}), leading to a higher specific detectivity (1.8×10^{12}Jones) when compared to the device with the PEDOT:PSS layer. We further investigated the Schottky barrier height of the ITO/MAPb $(I_{1-X}Br_X)_3$ interface by using capacitance-voltage (C-V) measurements.

In experiments, patterned ITO glass substrates (2 cm in length and width, 1 mm in height, with a piece of 2 mm in width, 2 cm in length patterned ITO in the middle) were cleaned in deionized water, acetone, and ethanol orderly in an ultrasonic bath for 15 min, and dried under nitrogen flow, followed by ultraviolet ozone treatment for 10 min. For the device with a PEDOT:PSS layer, PEDOT:PSS (Clevios 4083) was spin-coated on the substrates under 2000 rpm for 60 s and annealed at 150 °C for 20 min in air. Otherwise, the substrates were transferred directly to the glove box for device fabrication. The perovskite precursor (see supplementary information for experiment, available online at stacks.iop.org/SST/34/074004/mmedia) was spin-coated on the substrate at 3000 rpm for 40 s, with 200 μl chlorobenzene added on the substrate after the speed reaches 3000 rpm during the spin-

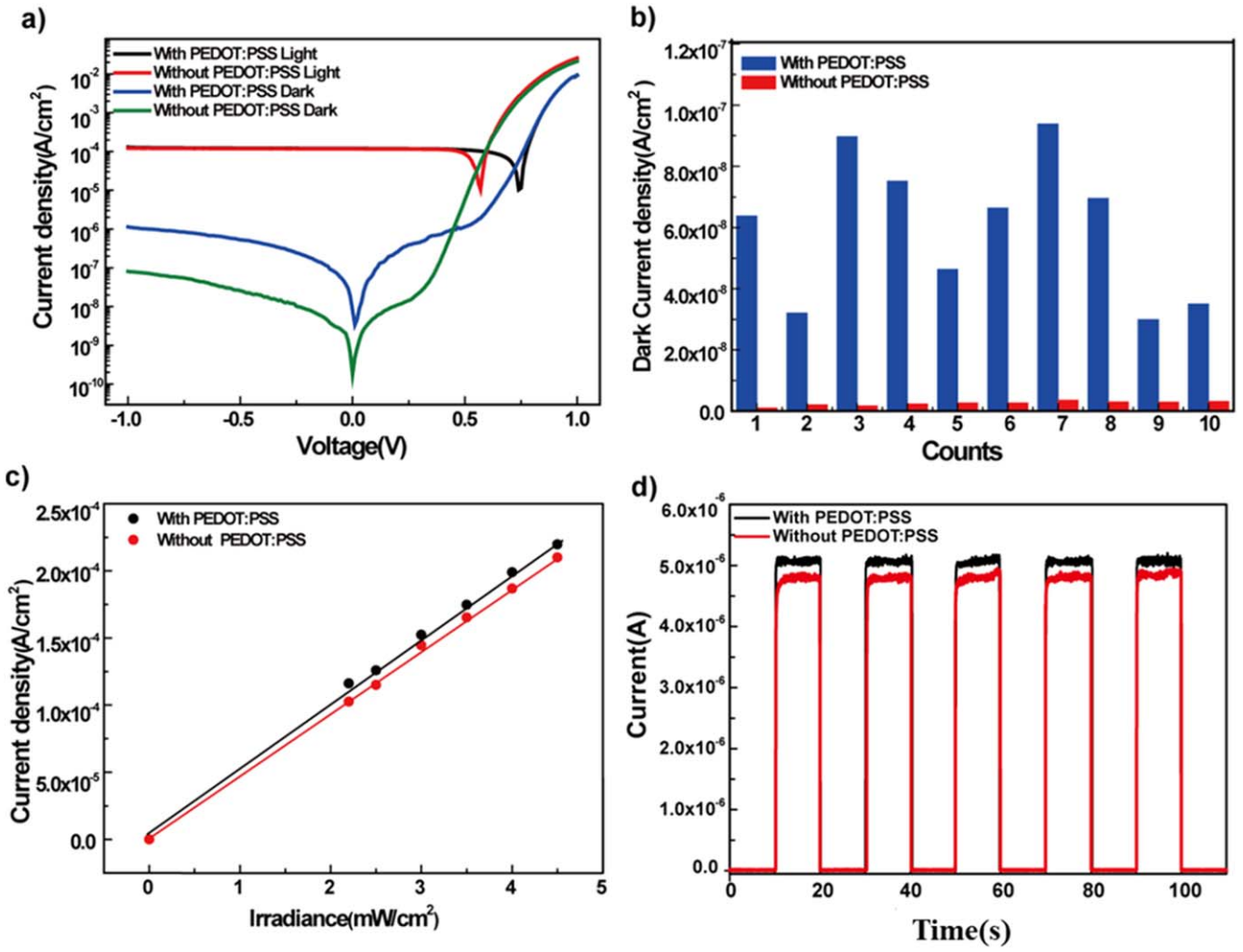

Figure 2. (a) J-V characteristics of devices in the dark and under light illumination at 500 nm with an intensity of 0.4 mW cm^{-2}. (b) Statistics of the dark current density of ten photodiode devices with and without a PEDOT:PSS layer when baised at −0.1 V. (c) Linear dynamic range of the devices. (d) Photocurrent rise and delay time of the devices.

coating process to decrease the crystallization time of perovskite to obtain smooth compact perovskite thin films [22]. The substrates were heated on a hot plate at 100 °C for 10 min to convert the spin coated film into a polycrystalline perovskite. Details of the perovskite material characterizations can be found in figure S1, available online. The PCBM solution was then spin-coated on the substrate at 2000 rpm for 40 s, followed by annealing at 100 °C for 10 min. Next, the BCP solution was spin-coated on the substrate at 2000 rpm for 60 s. Finally, the Ag electrode (80 nm) was thermally evaporated on the substrates through a shadow mask.

To investigate the performance of photodiodes, typical current density-voltage (J-V) curves of our best perovskite photodetectors with and without a PEDOT:PSS layer under dark and under illumination (0.45 mW cm^{-2} at 500 nm) conditions were plotted in figure 2(a). The photocurrent of both photodetectors, with or without a PEDOT:PSS layer, is almost equivalent to each other, which is around 1.2×10^{-4} A cm^{-2} at −0.1 V. Notably, the dark current of the device without a hole transporting layer is about one order magnitude lower than that of the device with a PEDOT:PSS layer, reaching 1.9 nA cm^{-2} at −0.1 V. As a result, the rectification ratio of the HTL free device reaches 10^5 when biased at ±1 V. The dark I–V characteristics of the fabricated photodetectors are quite reproducible. Statistics of the dark current densities of ten photodiode devices with and without a PEDOT:PSS layer were presented in figure 2(b), showing that an average of dark current of the PEDOT:PSS free device is about one order magnitude lower than the device with PEDOT:PSS. To access the photodiode's performance, the responsivities and detectivity were calculated. The responsivities (R) of the photodiode at 500 nm is ∼0.22 A W^{-1}, which is consistent with previously reported values [23]. The specific detectivity (D^*) is also evaluated according to the following equation [24]

$$D^* = \frac{R}{(2qJ_d)^{1/2}} \quad (1)$$

where R is the responsivity and q is the elementary charge. Due to the dark current difference, the HTL free device shows a much higher $D*$ while the two devices have similar R. The $D*$ of the devices are calculated to be 8.9×10^{12} Jones,

which is very close to the previously reported value found in electron transport layer modified perovskite photodiode evaluated by the same method [17]. It is worth noting that PEDOT:PSS is still favorable for solar cell applications, as shown in figure S2. The power conversion efficiency (PCE) of the device with PEDOT:PSS is higher than the device without a PEDOT:PSS layer. It suggests that under light bias, PEDOT:PSS acts as an effective hole transporting layer for extracting photo-generated holes from the perovskite layers, yet, when operated under dark, the PEDOT:PSS could not block the electron injection from the ITO electrode, leading to a high reverse saturation dark current at the PEDOT:PSS/perovskite interface.

The linear dynamic range (LDR), which shows how linear a response the detector has for different light intensities, is given by:

$$LDR = 20Log\frac{Jph\ \max}{Jd} \tag{2}$$

where $J_{ph\ \max}$ is maximum photocurrent within a linear range. The LDR of the device without the PEDOT:PSS layer is measured to be 101 dB, which is much higher than the LDR (69 dB) of the device with the PEDOT:PSS layer, as shown in figure 2(c). In contrast, the LDR of some inorganic photodetectors, such as InGaAs photodetectors, can only achieve 66 dB [25], and the LDR of the traditional Si photodetectors is around 120 dB. It is worth noting that our LDR is currently limited by the maximum light source intensity, which is not the intrinsic limit of the perovskite photodetector device.

Transient photocurrent behavior of both devices were also investigated and plotted in figure 2(d), which shows five-cycle curves of a photocurrent time response under an interval of 10 s illumination. Both the device with or without a PEDOT:PSS layer switch in a fast speed, where the rise times and delay times are less than 50 ms as indicated in figure S3. The transient behavior is currently limited by the sampling time of the test equipment, which is not the ultimate switching speed of the perovskite photodetector. The ON/OFF ratio of photodetectors without the PEDOT:PSS layer is 6.06×10^4, which is one order higher than the ON/OFF ratio (1.51×10^3) of the traditional structure at the bias of −0.1 V. The high photosensitivity value from the device without the PEDOT:PSS layer originated from its low dark current. Generally speaking, the origination of dark current in a diode is mainly composed of the recombination and injection of carriers under reverse bias. In order to reveal the origin of the lower dark current in the HTL free photodiode, we further perform EIS measurements to investigate the recombination of carriers in the dark.

An electrochemical workstation (CHI660E) with a frequency range from 0.1 MHz down to 1 Hz at a bias potential of 0.8 V (with a 5 mV sinusoidal AC perturbation) was employed for electrochemical impedance spectroscopy at room temperature in dark conditions. The Nyquist plot of the EIS measurement results is shown in figure 3(a). Considering the device structure, the equivalent circuit shown in the inset in figure 3(a) is used as a model. The series resistance component in the circuit model, R1, is associated with ITO resistance, and R2 indicates the parallel resistance of the device, which is related to its leakage current. By fitting the circuit model in figure 3(a), we can derive the R1 and R2 values. The results show that the device with the PEDOT:PSS layer has a smaller R1 (176.6 ohms) than that of the device without the PEDOT:PSS layer (230.2 ohms), suggesting that the PEDOT:PSS contact layer allows faster charge transfer at the interface than the ITO/perovskite interface. Nonetheless, it is worth noting that R2 obtained from the device without the PEDOT:PSS layer, 2.47×10^4 ohms, is larger than that of the device with PEDOT:PSS, 1.246×10^4 ohms. This suggests that PEDOT:PSS would induce more charge recombination under darkness in the device. As the perovskite layer is fabricated in the same manner, the main recombination pathway is suspected to be at the interface rather than in the bulk. We conclude that although PEDOT:PSS is beneficial for hole transportation, it does not serve as a good electron blocking layer, probably due to the indium defect in the PEDOT:PSS layer, which leads to charge recombination at the PEDOT:PSS/pervoskite interface. A possible dark current generation mechanism for the device with PEDOT:PSS is shown in figure 1(b). It is suspected that the acidic nature of PEDOT:PSS, with a pH value of ∼2, will lead to the corrosion of ITO, causing In ion diffusion into the PEDOT:PSS layer [26]. The defective In in the PEDOT:PSS would give rise to the intermediate states in the PEDOT:PSS which act as recombination centers for injected hole and electrons. In the dark and under reversed biased condition, the thermal generated holes from the perovskite will be transported to the PEDOT:PSS layer, where they recombine with the electron injected from ITO with the assist of In defect at the PEDOT:PSS/ITO interface. The injected holes and electron recombination then leads to the high dark current in devices with PEDOT:PSS, as shown in figure 1(b).

For the device without PEDOT:PSS, the injection of electrons is suspected to be mainly suppressed by the barrier height of the Schottky contact between ITO and perovskite. The Schottky junction at the ITO/perovskite interface should follow a typical Schottky diode equation

$$\mathrm{J} = J_0\left[\exp\left(\frac{qV}{nkT}\right) - 1\right],\ \text{and}\ J_0 = A^*T^2\exp\left(\frac{-q\phi_b}{kT}\right) \tag{3}$$

where J_0 is the dark reverse saturation current, a parameter that is directly related to the recombination rate in semiconductors [17], A is the Richardson constant, n is the ideality factor, V is the applied voltage and Φ_b is the Schottky barrier height. The dark J–V curve of the solar cells is then extrapolated to extract the dark saturation current density, J_0. As shown in figure 3(b), the HTL free device has a pretty low J_0 of 2.2×10^{-13} A cm^{-2}, which implies that the leakage current is successfully suppressed by the Schottky junction.

To further reveal the relationship between the dark current and the Schottky barrier height, Schottky type devices based on perovskite with different amounts of bromine (Br) substitution were fabricated. It is well known that the band gap of perovskite could be widened by increasing Br content, which would in return affect the Schottky barrier height at the

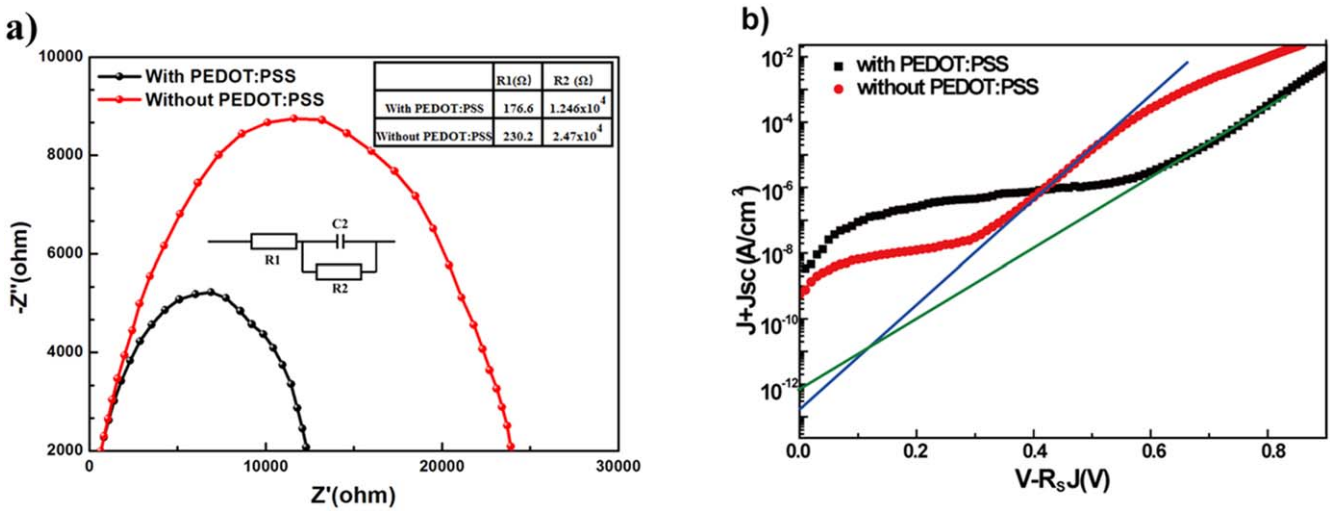

Figure 3. (a) Electrochemical impedance spectroscopy of the device. (b) Plot of ln(Jsc + J) versus (V-R_SJ) and the linear fitting for reverse saturation current extraction.

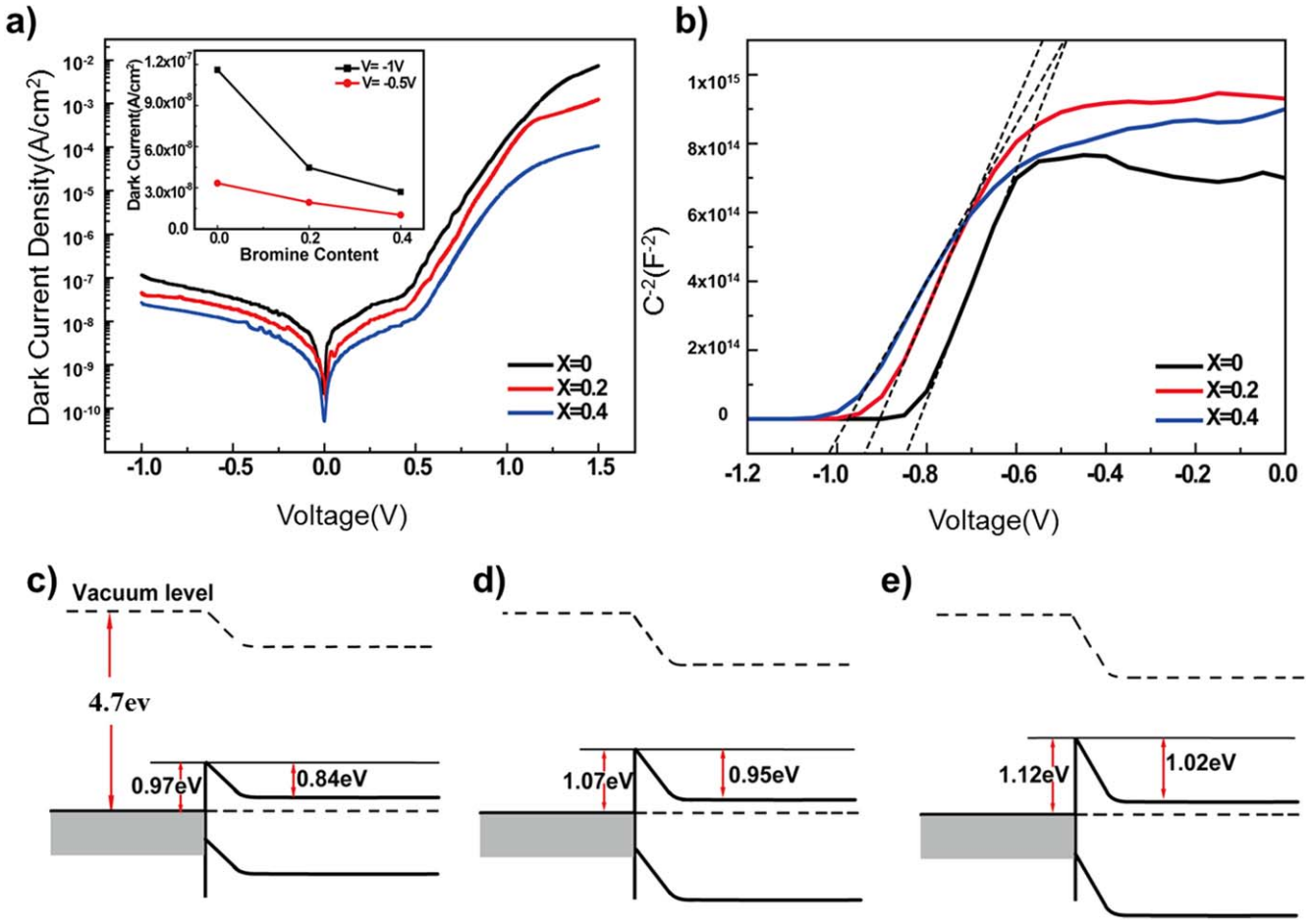

Figure 4. (a) Dark current of the device with different Br content. (b) C-V characteristics of the device measured at 1 kHz. (c)–(e) The energy diagram of ITO/MAPb $(I_{1-X}Br_X)_3$ contact (x = 0, 0.2, 0.4).

ITO/perovskite junction. The J-V curves of the fabricated devices with increasing Br content is presented in figure 4(a), with an inset plot highlighting the dark current values obtained at −1 V bias. It clearly shows that, when biased at −1 V, the dark current of the ITO/perovskite Schottky photodiode decreases from 10^{-7} A cm^{-2} to 3 × 10^{-8} A cm^{-2} as the Br content in the perovskite increases from x = 0 to x = 0.4. To evaluate the Schottky barrier height of the ITO/MAPb $(I_{1-X}Br_X)_3 (0 \leqslant X \leqslant 1)$ contact, capacitance-voltage (C-V) measurements were then carried out by an

Table 1. The ITO/MAPb $(I_{1-X}Br_X)_3$ Schottky diode device parameters extracted from C-V measurements with different Br content (x).

Items	X = 0	X = 0.2	X = 0.4
$N_L(cm^{-3})$	6.89×10^{18}	7.16×10^{18}	7.35×10^{18}
$N(cm^{-3})$	5.21×10^{16}	7.91×10^{16}	1.33×10^{17}
$V_1(eV)$	0.127	0.117	0.104
$V_2(eV)$	0.84	0.95	1.02
$\Phi_b(eV)$	0.967	1.067	1.124

electrochemical workstation (CHI660E) with a frequency of 1000 Hz and bias potentials range from −1.2 V to 1.2 V (with a step of 0.05 V) at room temperature in dark conditions. In Schottky diodes, the capacitance of the depletion layer can be expressed as equation (4) [27, 28]

$$C^{-2} = \frac{2(V_1 + V)}{q\varepsilon_s A^2 N} \tag{4}$$

where A is the area of the diode, ε_s is the dielectric constant, N is the doping concentration value of semiconductor materials, and V_1 is the diffusion potential at zero bias and is determined from the extrapolation of the linear C^{-2}-V plot (figure 4(b)) to the V axis. Therefore, the value of the barrier height can be obtained by the following equation:

$$\phi_b = V_1 + V_2 \tag{5}$$

where V_2 is the potential difference between the Fermi level and the bottom of the conduction band. As judged from figure 4(b), with a positive slope from the C^{-2}-V plots, the perovskite films fabricated in our research were found to be n-type [29]. Then, the V_2 can be obtained from the following relation:

$$V_2 = kTLn\left(\frac{N_L}{N}\right) \tag{6}$$

where k is the Boltzmann constant, T is the absolute temperature, N_L is the effective density of states at the conduction band edge [30, 31] and N is the doping concentration. The doping concentration values (N) of the perovskite layer can be derived from the slope of the linear C^{-2}-V plot (figure 4(b)), which gives a value of 5.21×10^{16} cm^{-3} for the $MAPbI_3$, in agreement with the previous report [29]. Using equations (5) and (6), we are able to calculate the barrier height of ITO/MAPb $(I_{1-X}Br_X)_3$. The calculated results are summarized in table 1. Based on these results, the energy diagrams of the ITO/MAPb $(I_{1-X}Br_X)_3$ junction can be sketched, as shown in figures 4(c)–(e). The barrier heights at the ITO/perovskite junction increased from 0.967 eV to 1.124 eV when the Br content x increased from 0 to 0.4, leading to a lower reversed dark current for devices with higher Br content in figure 4(a). All of the above results suggest that there is a Schottky contact between the ITO and perovskite for the device without PEDOT:PSS.

In summary, the ITO/$CH_3NH_3PbI_3$ junction effectively suppresses electron injection from ITO to the perovskite under reversed bias, leading to a surprisingly low dark current of 1.9×10^{-9} A cm^{-2}. When functioned as a photodetector, the ITO/$CH_3NH_3PbI_3$ Schottky diode outperforms the conventional p-i-n perovskite photodiode with a PEDOT:PSS layer in terms of detectivity, reaching a high photosensitivity of 6.06×10^4 and a specific detectivity (D^*) of 8.9×10^{12} Jones. Moreover, the Schottky barrier height at the ITO/perovskite junction can be further adjusted by tuning the band gap of perovskite with the content of bromine. This work fundamentally reveals the device physics of Schottky diode based on the perovskite and transparent conductor, and provides a low cost technology solution for high sensitivity photodetectors.

Acknowledgments

This work is financially supported by the National Key Research and Development Program of China (2016YFA0202002), and Shenzhen Science and Technology Innovation Commission (JCYJ20160229122349365) is acknowledged. Chuan Liu would like to acknowledge Science and Technology Program of Guangdong Province (Grant No. 2015B090924001), Guangdong Natural Science Funds for Distinguished Young Scholars (Grant No. 2016A030306046)

ORCID iDs

Qing Dai https://orcid.org/0000-0002-1750-0867
Jun Chen https://orcid.org/0000-0001-7397-2714
Hang Zhou https://orcid.org/0000-0002-0472-9515

References

[1] Chen K-J, Hung F-Y, Chang S-J and Young S-J 2009 Optoelectronic characteristics of UV photodetector based on ZnO nanowire thin films *J. Alloys Compd.* **479** 674–7
[2] Fortunato E, Pereira L, Aguas H, Ferreira I and Martins R 2005 Flexible a-Si:H position sensitive detectors *Proc. IEEE* **93** 1281–6
[3] Stiff A D, Krishna S, Bhattacharya P and Kennerly S W 2001 Normal-incidence, high-temperature, mid-infrared, InAs-GaAs vertical quantum-dot infrared photodetector *IEEE J. Quantum Electron.* **37** 1412–9
[4] Fann S-S, Jiang Y-L and Hwang H-L 2003 Operating principles and performance of a novel a-Si:H pin-based x-ray detector for medical image applications *IEEE Trans. Electron Devices* **50** 341–6
[5] Ponseca C S Jr, Savenije T J, Abdellah M, Zheng K, Yartsev A, Pascher T R, Harlang T, Chabera P, Pullerits T and Stepanov A 2014 Organometal halide perovskite solar cell materials rationalized: ultrafast charge generation, high and microsecond-long balanced mobilities, and slow recombination *J. Am. Chem. Soc.* **136** 5189–92
[6] Heo J H, Im S H, Noh J H, Mandal T N, Lim C-S, Chang J A, Lee Y H, Kim H-j, Sarkar A and Nazeeruddin M K 2013 Efficient inorganic–organic hybrid heterojunction solar cells containing perovskite compound and polymeric hole conductors *Nat. Photon.* **7** 486

[7] Yusoff A R b M and Nazeeruddin M K 2016 Organohalide lead perovskites for photovoltaic applications *J. Phys. Chem. Lett.* **7** 851–66
[8] Noh J H, Im S H, Heo J H, Mandal T N and Seok S I 2013 Chemical management for colorful, efficient, and stable inorganic–organic hybrid nanostructured solar cells *Nano Lett.* **13** 1764–9
[9] Deng H, Yang X, Dong D, Li B, Yang D, Yuan S, Qiao K, Cheng Y-B, Tang J and Song H 2015 Flexible and semitransparent organolead triiodide perovskite network photodetector arrays with high stability *Nano Lett.* **15** 7963–9
[10] Chen S, Teng C, Zhang M, Li Y, Xie D and Shi G 2016 A flexible UV–Vis–NIR photodetector based on a perovskite/conjugated-polymer composite *Adv. Mater.* **28** 5969–74
[11] Hu X, Zhang X, Liang L, Bao J, Li S, Yang W and Xie Y 2014 High-performance flexible broadband photodetector based on organolead halide perovskite *Adv. Funct. Mater.* **24** 7373–80
[12] Casaluci S, Cinà L, Matteocci F, Lugli P and Di Carlo A 2016 Fabrication and characterization of mesoscopic perovskite photodiodes *IEEE Trans. Nanotechnology* **15** 255–60
[13] Wang Y, Xia Z, Du S, Yuan F, Li Z, Li Z, Dai Q, Wang H, Luo S and Zhang S 2016 Solution-processed photodetectors based on organic–inorganic hybrid perovskite and nanocrystalline graphite *Nanotechnology* **27** 175201
[14] Jung H S and Park N G 2015 Perovskite solar cells: from materials to devices *Small* **11** 10–25
[15] Wang C and Yang J 2016 Interface modification for organic and perovskite solar cells *Sci. China Mater.* **59** 743–56
[16] Huang F, Pascoe A R, Wu W Q, Ku Z, Peng Y, Zhong J, Caruso R A and Cheng Y B 2017 Effect of the microstructure of the functional layers on the efficiency of perovskite solar cells *Adv. Mater.* **29** 1601715
[17] Dou L, Yang Y M, You J, Hong Z, Chang W-H, Li G and Yang Y 2014 Solution-processed hybrid perovskite photodetectors with high detectivity *Nat. Commun.* **5** 5404
[18] Dong R, Fang Y, Chae J, Dai J, Xiao Z, Dong Q, Yuan Y, Centrone A, Zeng X C and Huang J 2015 High-gain and low-driving-voltage photodetectors based on organolead triiodide perovskites *Adv. Mater.* **27** 1912–8
[19] Nathan A, Park B, Sazonov A, Tao S, Chan I, Servati P, Karim K, Charania T, Striakhilev D and Ma Q 2000 Amorphous silicon detector and thin film transistor technology for large-area imaging of X-rays *Microelectron. J.* **31** 883–91
[20] Hou F, Jin F, Chu B, Su Z, Gao Y, Zhao H, Cheng P, Tang J and Li W 2016 Hydrophobic hole-transporting layer induced porous PbI2 film for stable and efficient perovskite solar cells in 50% humidity *Sol. Energy Mater. Sol. Cells* **157** 989–95
[21] Jeng J Y, Chiang Y F, Lee M H, Peng S R, Guo T F, Chen P and Wen T C 2013 $CH_3NH_3PbI_3$ perovskite/fullerene planar-heterojunction hybrid solar cells *Adv. Mater.* **25** 3727–32
[22] Salim T, Sun S, Abe Y, Krishna A, Grimsdale A C and Lam Y M 2015 Perovskite-based solar cells: impact of morphology and device architecture on device performance *J. Mater. Chem.* A **3** 8943–69
[23] Perini C A R, Barker A J, Sala M, Petrozza A and Caironi M 2018 High speed solution-processed hybrid perovskite photodetectors with low dark current enabled by a low temperature metal oxide interlayer *Semicond. Sci. Technol.* **33** 7
[24] Gong X, Tong M, Xia Y, Cai W, Moon J S, Cao Y, Yu G, Shieh C-L, Nilsson B and Heeger A J 2009 High-detectivity polymer photodetectors with spectral response from 300 nm to 1450 nm *Science* **325** 1665–7
[25] Sefunc M A, Pollnau M and García-Blanco S M 2013 Low-loss sharp bends in polymer waveguides enabled by the introduction of a thin metal layer *Opt. Express* **21** 29808–17
[26] Wong K W, Yip H L, Luo Y, Wong K Y, Lau W M, Low K H, Chow H F, Gao Z Q, Yeung W L and Chang C C 2002 Blocking reactions between indium-tin oxide and poly (3,4-ethylenedioxythiophene):poly(styrene sulphonate) with a self-assembly monolayer *Appl. Phys. Lett.* **80** 2788
[27] Weaver J H 1991 *Formation and Properties of Metal–Semiconductor Interfaces* (Berlin: Springer)
[28] Sze S 1981 *Physics of Semiconductor Devices* (New York: John Wiley) pp 122–9
[29] Wang Q, Shao Y, Xie H, Lyu L, Liu X, Gao Y and Huang J 2014 Qualifying composition dependent p and n self-doping in $CH_3NH_3PbI_3$ *Appl. Phys. Lett.* **105** 163508
[30] Zhou Y and Long G 2017 Low density of conduction and valence band states contribute to the high open-circuit voltage in perovskite solar cells *J. Phys. Chem.* C **121** 1455–62
[31] Chen Q, De Marco N, Yang Y M, Song T-B, Chen C-C, Zhao H, Hong Z, Zhou H and Yang Y 2015 Under the spotlight: the organic–inorganic hybrid halide perovskite for optoelectronic applications *Nano Today* **10** 355–96